J Mater Sci (2007) 42:6027–6035
DOI 10.1007/s10853-006-1149-6

Preparation, characterization and photocatalytic activity of TiO_2 / Methylcellulose nanocomposite films derived from nanopowder TiO_2 and modified sol–gel titania

Mohammad Hossein Habibi · Mojtaba Nasr-Esfahani · Terry A. Egerton

Received: 3 April 2006 / Accepted: 16 October 2006 / Published online: 6 April 2007

Abstract TiO_2—methylcellulose (MC) nanocomposite films processed by the sol-gel technique were studied for phocatalytic applications. Precalcined TiO_2 nanopowder was mixed with a sol and heat treated. The sol suspension was prepared by first adding titanium tetra isopropoxide ($Ti(OPr)_4$ or TTP) to a mixture of ethanol and HCl (molar ratio TTP:HCl:EtOH:H_2O = 1:1.1:10:10) and then adding a 2 wt.% solution of methylcellulose (MC). The TiO_2 nanopowder was dispersed in the sol and the mixture was deposited on a microscope glass slide by spin coating. Problems of film inhomogeneity and defects which caused peeling and cracking during calcinations, because of film shrinkage, were overcome by using MC as a dispersant. Effect of MC on the structure evaluation, crystallization behavior and mechanical integrity with thermal treatment up to 500 °C are followed by SEM, XRD and scratch test. XRD Scanning electron microscopy (SEM) showed that the composite films with MC have much rougher surface than films made without MC. Composite films heat treated at approximately 500 °C have the greatest hardness values. For the composite thick film, the minimum load which caused the complete coating removal was 200 g/mm^2, an indication of a strong bond to the substrate. Photocatalytic activities of the composite film were evaluated through the degradation of a model pollutant, the textile dye, Light Yellow X6G (C.I. Reactive Yellow 2) and were compared with the activity of (i) a similar composite film without MC, and (ii) a TiO_2 nanopowder. The good mechanical integrity make this composite film an interesting candidate for practical catalytic applications.

M. H. Habibi (✉) · M. Nasr-Esfahani
Department of Chemistry, University of Isfahan, Isfahan 81746-73441, Iran
e-mail: habibi@chem.ui.ac.ir

T. A. Egerton
School of Chemical Engineering and Advanced Materials, University of Newcastle upon Tyne, Bedson Building, Newcastle NE1 7RU, UK

Introduction

Most of the synthetic dyes used for paper, printing and textiles are released into the environment [1–3]. For azo dyes, the largest class of dye used for cotton, the most widely used fabric [4, 5], up to 30% is unfixed to the fabric and is discharged. These azo dyes are highly light-stable and resistant to microbial attack and the electron withdrawing nature of the N=N bond lowers their susceptibility to aerobic oxidation [6]. Therefore, they are neither readily degraded nor removed by conventional wastewater treatment. Further, their hydrophilicity limits removal by coagulation/flocculation, which, in any case, produces large amounts of sludge with consequent disposal problems. However, since even low levels are clearly visible and exert a significant environmental impact, it is necessary to develop effective treatment methods.

Heterogeneous photocatalysis, one of the advanced oxidation processes (AOPs) of particular interest for the degradation of organic pollutants, uses large band gap semiconductors, particularly TiO_2 and UV light to cleave the azo bond and decolorize the dye [7–17]. It has been shown that TiO_2, particularly anatase, slurries can cause complete mineralization of organic pollutants. This is important because aromatic amines derived from partial oxidation of azo dyes may be toxic or carcinogenic [12]. However, because of high fixed and variable costs, numerous attempts to improve the photocatalytic activity of

TiO_2 by modifying the surface or bulk properties, by e.g., doping, codeposition of metals, surface chelation, mixing of two semiconductors, etc. have been reported [18–20]. It is clear that recombination of the initially generated charge-carrier is one of the most important factors that must be minimized to achieve high photocatalytic activity [21–23].

Because the use of slurries necessitates separation of the catalyst from the treated liquid, immobilization of the TiO_2 has received much attention. Although sintering of colloidal TiO_2 paste is the simplest way to fabricate porous films, the low mechanical integrity of such films makes them unsuitable for large scale applications. Alternative routes to nanostructured TiO_2 films include electron-beam evaporation, magnetron sputtering, anodization, chemical vapor deposition and sol–gel methods. The sol–gel techniques offer options of varying the film properties and controlling product homogeneity, purity, microstructure whilst avoiding excessive process costs and many reports describe the fabrication of sol–gel TiO_2 films by dip coating with precursors derived from titanium alkoxides. The major disadvantage is shrinkage of the resulting product (film or monolith) during drying and heat treatment [23–27]. Mechanical integrity may be a particular problem with thick films, but as thin (<200 nm) films may exhibit relatively low photoefficiency the use of polymerized materials to improve homogeneity, increase surface area and improve adhesion/cracking after calcination has been explored. A processing method to produce sol–gel derived composite-coatings of photocatalytic TiO_2 without any dispersant has also been reported [27–37].

This study, part of a programme to develop solid films for photocatalytic and photoelectrocatalytic purposes [38–40], describes the preparation of novel composite films derived from TiO_2 sol–gel and nanopowder using methylcellulose (MC), a non-ionic water-soluble long chain polymer, as dispersant. We have used a high surface area TiO_2 in order to reduce the decrease in surface area associated with densification and crystal growth of the filler and/or matrix in the composite. By using MC as a dispersant we have solved some problems like inhomogeneity and defects that may induce peeling and cracking after calcination due to film-shrinkage on thermal treatment. Not only is MC suitable for use in sol–gel processing but in addition it is not likely to promote crystallization of titania during any of the coating, formation, and densification process steps [37, 41]. Indeed, non-ionic polymers are reported to produce smaller grains, perhaps by retarding crystallization of titania.

The films were deposited on glass substrates by spin-coating and their photocatalytic activity for the decolorization of a textile dyes—Light Yellow X6G (C.I. Reactive Yellow 2)—was evaluated as a function of dye concentration and solution pH and compared with a similar, MC-free, composite film and with TiO_2 nanopowder.

Experimental

Materials

Ethanol (Fluka, 99.8%) 35.5% hydrochloric acid (Merck) and titanium tetra-isopropoxide (TTP) (Aldrich, 97% $Ti(O^iPr)_4$) were used without further purification. The TiO_2, anatase nanopowder is stated by Aldrich to have a surface area of 190–290 $m^2\ g^{-1}$ and a particle size of ~15 nm. Methylcellulose (low substitution) was obtained from Harris Chemical. Light Yellow X6G dye has the chemical structure shown in Fig. 1 (C.I. Reactive Yellow 2, RMM 872.5) and was obtained from Youhao (China). Solutions were made up in doubly distilled deionized water.

Preparation of thin film

The reagents were used as received. Anhydrous ethyl alcohol (EtOH) was used as the solvent because the water content of the sol has a critical role in the hydrolysis and polycondensation reactions. A titania solution containing organic binder material MC was made using the following procedure. First, 5 mL TTP was dissolved in a mixture of 10 mL ethanol and 1.8 mL HCl 35.5 wt.%, and the solution was agitated for homogenization. In a separated container, methylcellulose solution (2 wt.% in water) was prepared by dissolving 0.02874 g of MC in 1.4 mL double distilled water. Then these two solutions (titanium precursor and MC solution) were added dropwise and stirred overnight at room temperature. The mole ratio was TTP:HCl:EtOH:H_2O, 1:1.1:10:10. Spin-coating technique was used to deposit the sol onto the substrate surface (microscope glass slide). Drops of the mixture were deposited on the surface of the glass slide with spinning. After drying at room temperature in the air, the films were heated for about 1 h at 500 °C to study optical transmit-

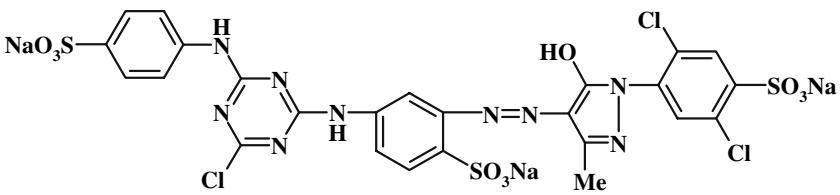

Fig. 1 Chemical structure of commercial diazo dye, light Yellow X6G (C.I. Reactive Yellow 2)

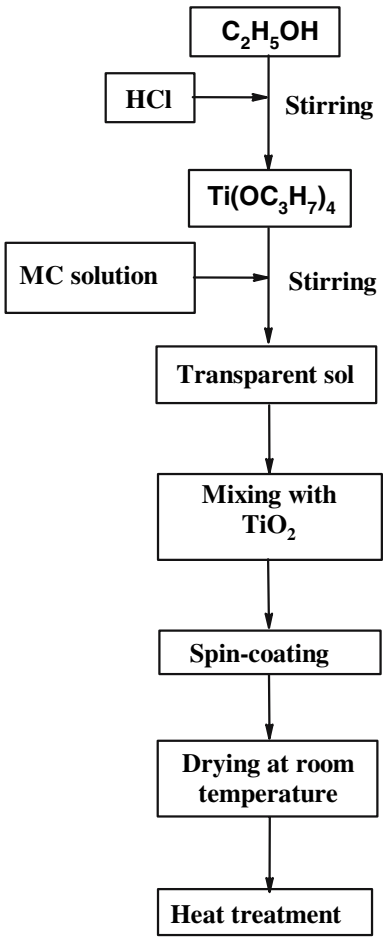

Fig. 2 Preparation of composite TiO_2 film coating

tance spectra and detect absorption edges of the films (Fig. 2). For comparison, the similar sol without MC was prepared and deposited onto microscope glass slide.

Preparation of sol–gel composite film

The Aldrich TiO_2 nanopowder was dispersed in the sol as a filler at a level of 5% (w/w) and the additioned mixture was deposited on a microscope glass slide (75 mm × 25 mm × 1 mm; ultrasonically cleaned in ethanol) by spin coating for 30 s at 2,000 rpm. The films were dried and heated at 5°C min^{-1} in a muffle furnace to 500 °C and held at this temperature for 60 min before cooling at about 5°C min^{-1} to room temperature. Prior to use in photocatalytic experiments the films were stored in the dark.

Characterization techniques

The structure and crystallite size were determined by powder X-ray diffraction (Bruker D8 Advanced X-ray diffractometer: Cu Kα radiation; scan rate 0.03 2θ s^{-1}). The mean crystallite sizes of TiO_2 were calculated by Scherrer's equation using the full width at half maximum (FWHM) of the X-ray diffraction peaks at $2\theta = 25.3°$.

TGA measurements were made, using a Mettler TA5 instrument, on the powder obtained by pouring a mixture of sol and TiO_2 nanopowder into a Petri dish and then drying at room temperature for ~10 days. About 0.01 mg samples of the crushed powder were heated in an Al_2O_3 crucible at 5 °C min^{-1} from room temperature to 700 °C in flowing air. Similar measurements were made on the MC.

The mechanical integrity of spun coatings of the same controlled thickness was measured using a motorized Clemen scratch tester equipped with a tungsten carbide 1 mm ball tool. Scratches were made under an applied load which increased from 0 to 1,000 g over a 50 mm length. The load at which the indenter started to scratch the substrate surface was identified visually and considered as indicative of the coating resistance to scratch failure.

The stability of TiO_2 suspensions was investigated by sedimentation in 50 mL, ~20 mm diameter, measuring cylinders. The suspensions were poured into cylinders to the exact height of 20 cm and the sedimentation distance was measured with time.

The microstructure of the (gold sputtered) composite films was observed by Scanning Electron Microscopy (SEM) Philips XL30, operated at 20 kV.

Photoreactor and photocatalytic measurements

The photocatalytic degradation experiments were carried out with10 mL solution in a reactor with total volume 40 mL and placed in a 25 °C water bath. A singly coated slide (75 mm × 25 mm × 1 mm) was irradiated by two 8 W UVA (Philips, $\lambda = 365$ nm) lamps placed 5 cm above the solution. In a typical experiment, each dye solution with initial concentration of 12 mg dm^{-3} was stirred continuously and 10 mL samples were taken at regular intervals during irradiation and analyzed by UV–visible spectroscopy (Varian Cary 500 Scan double beam spectrophotometer) to monitor the photocatalytic degradation of dye at 270.0 nm. Control experiments were also carried out using TiO_2 nanopowder suspension 160 mg dm^{-3} slurry under the same conditions.

Results and discussion

Preparation of sol

Different compositions of TiO_2 sol were prepared by altering the molar ratio of TTP:H_2O:HCl. The typical sol, reported here, with TTP:H_2O:EtOH:HCl molar ratio of 1:10:10:1.1, was found to be most suitable for dissolving MC and dispersing TiO_2. Increasing the water content and dilution of

the sol system, may retard the gelation process. The process was exothermic and the pH of the solution about 2–3.

Stability of suspensions of anatase nanopowders in the sol

The sedimentation rates of TiO_2 nanopowder dispersed in the alkoxide derived sol were taken as an indication of their degree of dispersion [42]. MC addition increased the sedimentation time of 5% (w/w) powder dispersions from 1 to 70 h. and of the 10% (w/w) powder from 0.5 to 10 h. Although the increased viscosity of the MC additioned fluid will lower sedimentation rates, the decreased sedimentation rate is believed to be associated primarily with the better dispersion of the nanopowders that results from their steric stabilization by MC.

Thermogravimetric analysis

Thermogravimetric analyses (TGA) [of the gel powders of the composite materials obtained from the mixed sol solution with TiO_2 nanopowder] showed weight losses at

(a) below 200 °C—considered to be due to loss of water and the thermal decomposition of residual organic solvents,
(b) from 200 to 280 °C attributed to the carbonization or the combustion of organic compounds, e.g. MC in the composite and
(c) from 280 to 450 °C probably due to dehydroxylation of the TiO_2 and combustion of the residual organic additives.

XRD characterization of TiO_2 photocatalyst

The XRD patterns of the gel-derived powders of sample A (the sol without MC), heat treated for 1 h at different temperatures in air, is shown in Fig. 3a. The as-prepared gel have amorphous structure, showing a very broad peak at about $2\theta = 25.2°$ (which is identified as the most intensive peak (1 0 1) for the anatase TiO_2). In general, the hydrolysis products in the sol–gel processing do not show crystallinity on XRD spectrum. By increasing the calcinations temperature, the (1 0 1) peak of anatase has become sharper, which indicates the dependence of crystallinity to

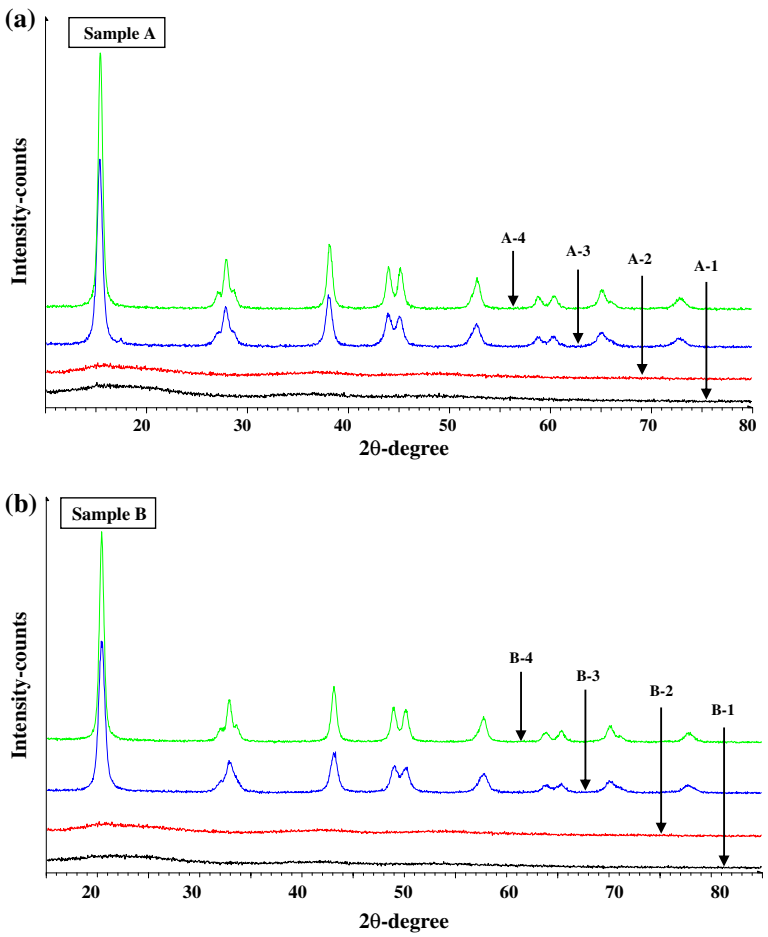

Fig. 3 X-ray diffraction patterns of the samples listed in Table 1 (heat treated at different conditions). (**a**) Sample A: sol–gel-derived TiO_2 powder without MC, as-prepared (A-1) and heat treated for 1 h at: 125 (A-2), 300 (A-3), 500 °C (A-4). (**b**) Sample B: sol–gel-derived TiO_2 powder with MC, as-prepared (B-1) and heat treated for 1 h at: 125 (B-2), 300 (B-3), 500 °C (B-4)

Table 1 Physical characteristics of different TiO_2 photocatalysts heat treated for 1 h at different temperatures, the crystallite size and adhesion strength

Material	Code	Heat treatment condition (°C)	Crystallite size (nm)	Scratch adhesion (g/mm2)[a]
Sample A[b]	A-1	–	0.7	150
	A-2	125	0.7	–
	A-3	300	5.1	–
	A-4	500	15.5	1,500
Sample B[c]	B-1	–	0.6	160
	B-2	125	0.6	–
	B-3	300	5.0	–
	B-4	500	13.4	1,500
Nanopowder	C-1	–	15	~0
TiO_2	C-2	500	16.3	~0
Composite	D-1	–	15.0	9
TiO_2 film[d]	D-2	500	16.4	200

[a] Critical linearly increasing loads

[b] Thin film of TiO_2 without MC

[c] Thin film of TiO_2 with MC

[d] Prepared from 5 wt.% Aldrich nanopowder TiO_2 in the sol

the applied temperature which happens at temperature lower than 300 °C. The corresponding crystallite size of the anatase in the heated powder is presented in Table 1. This is in accordance with the reported results of the calcination of the sol–gel-derived TiO_2, at different thermal conditions [43]. As shown in Fig. 3a and Table 1, for sample A, the crystallite size of anatase phase, used as a measure of TiO_2 crystallinity, increased markedly with calcination temperature, up to 15.5 nm at 500 °C. It is suggested that the growth process of nanocrystalline anatase is due to the sintering of the single crystals within the agglomerates, and finally the original agglomerate transforms to a larger single crystal [44].

The same observations, as shown in Fig. 3b, were carried out for the gels prepared from sample B (the sol with MC). It can be observed that the crystal formation and the polymorphs evolution in the sol with MC, upon heat treatment, are approximately the same as the sol without MC. As shown in Table 1 the crystal size of anatase TiO_2 at 500 °C was decreased to 13.3 nm in sol with introducing MC. In other words, for the sol system in this study, organic binder MC was found to be very suitable due to its lack of particle aggregation. Therefore, MC was introduced into the sol–gel precursors in addition to adjusting the viscosity of the sol for increasing the strength of the unfired materials, and preventing film crack formation. Another advantage of using MC as binder is that it belongs to non-ionic cellulose ether material and substantially free of substance that can induce crystallization of titania.

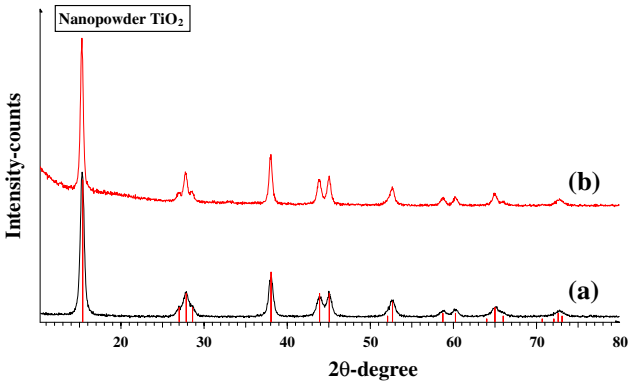

Fig. 4 X-ray diffraction patterns of the nanopowder TiO_2 (**a**) as-received and (**b**) heat treated for 1 h at 500 °C

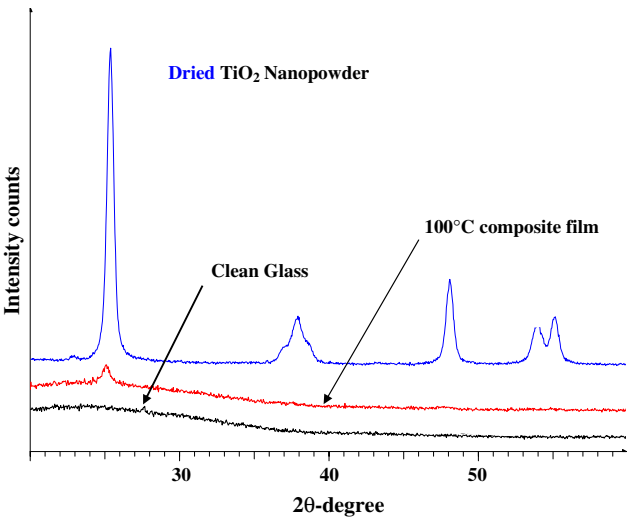

Fig. 5 XRD diffractograms of clean glass, dried TiO_2 nanopowder, and coated glass resulting from one spin-coating of the TiO_2 composite, prepared with MC addition and dried at 100 °C

Figure 4 illustrates XRD patterns of nanopowder TiO_2, as received and after calcination for 1 h at 500 °C. Nanopowder TiO_2 as-received powder contains ~100% anatase. Heating of this powder, even up to 900 °C (not shown here), did not result in the formation of rutile and the maximum detected rutile content remains at about 3%, perhaps due to fewer nucleation sites for rutile. Nanopowder TiO_2 anatase crystallites grow 20–30% compare to its original size when heated to 500 °C.

Figure 5 shows XRD spectrum of clean glass, dried TiO_2 nanopowder, and composite/glass with one time of spin-coating and dried at 100 °C. The diffractogram (Fig. 5) of the dried TiO_2 powder showed very clear and intense anatase peaks compared with the XRD pattern for TiO_2 composite film heated to 100 °C (as expected the clean glass show only a broad band at a d value of 3.50 nm).

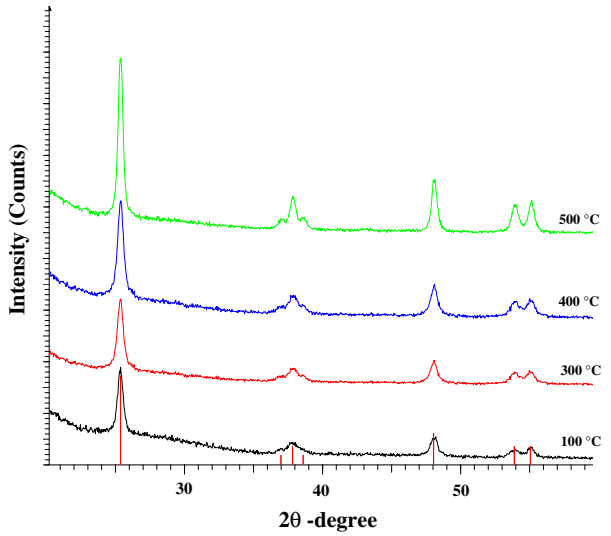

Fig. 6 The effect of increasing temperature on the diffraction patterns of TiO_2 composite films, prepared with MC addition, resulting from one spin-coating

The diffractograms of the composites prepared from anatase nanopowder dispersed in the alkoxide sols after heating to increasing temperatures are shown in Fig. 6. These diffractograms were measured at higher sensitivity than those in Fig. 5 as shown by the apparently more intense peaks of the film heated at 100 °C. Again, all peaks (2θ = 25.28°, 37.02°, 37.80°, 38.82°, 48.05°, 53.9°, and 55.06°) correspond to known diffraction maxima of anatase, and all intensities grew as the heating temperature was increased from 100 to 500 °C.

These changes are consistent with reports by Mazzarino et al. [45] and Keshmiri et al. [33] of the conversion of an amorphous titania thin film into anatase by treatment at 500 °C. They also agree well with Harizanov and Harizanova's [46] observation that changes between 250 and 550 °C in the exotherms of TiO_2 gel reflect the oxidation of the organic residues and consequent crystallization of the anatase form of TiO_2.

As shown in Table 1, typical values of anatase crystallite size of the synthesized TiO_2 particles on glass were 16.5 ± 0.5 nm. It is noteworthy that the size of the crystallites derived from the sol–gel is so similar to the size of the anatase nanoparticles.

Surface morphology

Figure 7a and b shows the SEM images of the composite film with thermal annealing at 500 °C for 60 min. In Fig. 7a it can be found that crevice in nanoscale appeared on the surface of coatings with introducing MC. Figure 7b shows the SEM image of composite film without MC which shows large cracks and some flaking off.

Figure 7c demonstrates the nanostructure of composite film and shows particle size of TiO_2 in SEM image correspond with XRD results.

Scratch adhesion test

The results of four repeated scratch adhesion tests (Table 1) showed that introduction of nanopowder TiO_2 caused a decrease in the adhesion and bonding strength between

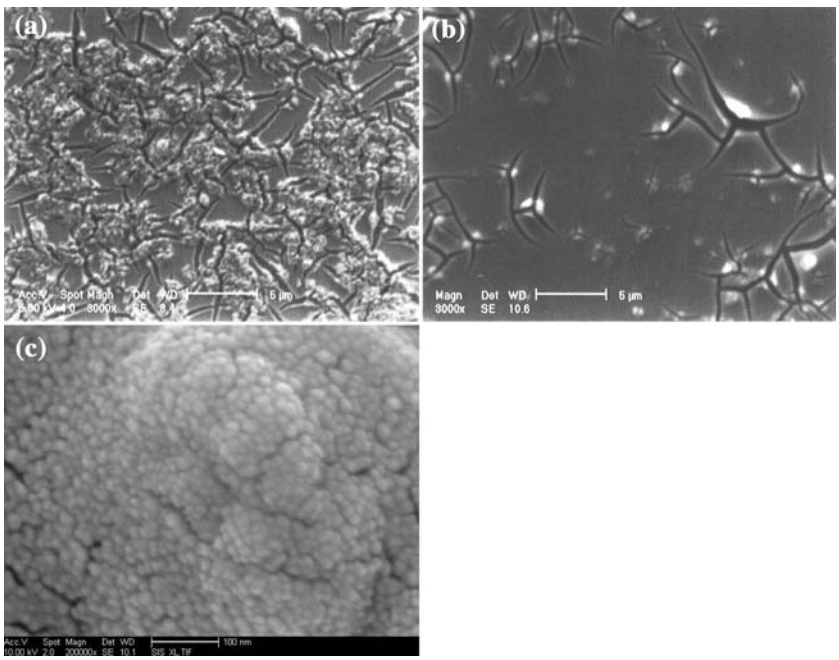

Fig. 7 SEM images of the composite TiO_2 film after heat treatment at 500 °C (**a**) with MC (**b**) without MC and (**c**) high magnification micrograph of composite film with MC

the thin film coating and the glass substrate. For the non-porous rigid coatings, such as thin film TiO_2 deposited on the glass substrate, the failure of the coating is sudden and accompanied by the breakage and separation of the coating from the substrate. However, for the case of porous composite films, the mechanical failure (i.e. peeling of the coating) dose not happen upon a certain critical load (i.e. it is not sudden). Therefore, the mechanical failure can not be defined as a point at which the detachment occurs and so the normal loads which caused the complete coating removal, for TiO_2 thin, nanopowder and composite films, within the scratch track (observed by optical microscope) are shown in Table 1. On the other hand the results indicate that when the organic binder material MC, a stimulating addition for structure control, is integrated in the inorganic system, low shrinkage, and high crack-resistance of the composite material are achieved because the bulky organic components fill the pores between the inorganic oxide chains and strengthen the gel network, probably by neck growth, which is in accordance with XRD and SEM results.

Optical transmittance

Figure 8 shows the UV–vis transmittance (T %) spectra of the TiO_2 films on the microscope slides in the wavelength range of 300–800 nm. In the visible region, and specifically at 565 nm, transmittance for the composite film with MC was 9%, while that of TiO_2 thin film prepared without MC and with MC were 83% (without nanopowders TiO_2), and the microscope slide (glass substrate) was about 91%. It is clear that the use of MC did not affect the transmittance but transmittance of composite film with nanopowder TiO_2 show sharp decrease.

At about 380 nm the transmittance decreases quickly for all films and approaches zero at around 330 nm. This fast decrease in the transmittance is due to absorption of light caused by the excitation and migration of electrons from the valence band to the conduction band of TiO_2. From Fig. 6 it is observed that the well-defined absorption edge changes slightly as the film thickness is increased (for composite film).

Photocatalytic activity

Evaluation of the films as potential photocatalysts for water pollutant purification was based on the discoloration of the model azo dye, X6G. Preliminary experiments demonstrated that in the absence of TiO_2, X6G was not degraded by 12 h UV irradiation and that dye-degradation was insignificant in the dark. However a small contribution to the decoloration is due to adsorption of the dye onto TiO_2 glass supported film. As this adsorption is expected to depend on the pH-dependent surface charge of the TiO_2, experiments were carried out at pH 5.1 the reported p.z.c. of the nanosized TiO_2 [47]. At this pH adsorption of the dye onto the TiO_2 composite/glass was negligible.

UV irradiation of all TiO_2 materials—slurry or composite film with or without MC—resulted in an effective photocatalytic decomposition of the azo dye. To a first approximation the three modes of degradation (i.e. slurry TiO_2 and two composite films) follow pseudo first-order reaction kinetics, i.e. plots of $\ln(C_0/C)$ versus time in the optimized conditions were linear (Fig. 9). This is consistent with, but does not prove, the generally held view that photodegradation rates of chemical compounds on semiconductor surfaces follow the Langmuir-Hinshelwood model [48, 49]. The pseudo first-order reaction rate constants and half-life parameters are listed in Table 2.

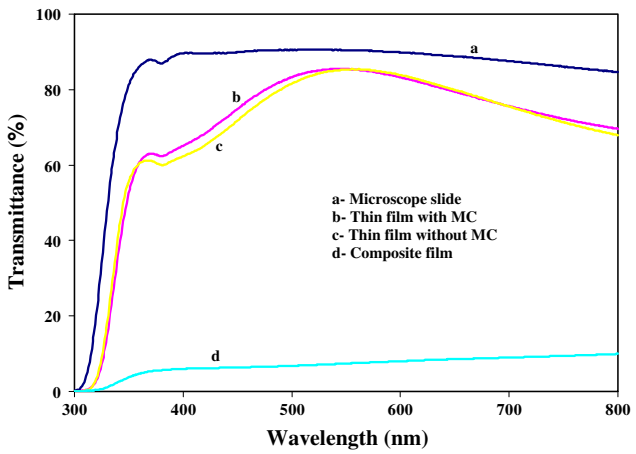

Fig. 8 Optical transmittance (T %) of the composite TiO_2 film, thin film of TiO_2 with and without MC

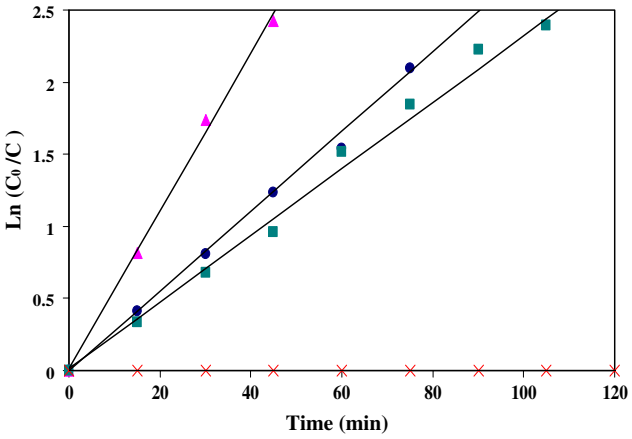

Fig. 9 The kinetic data for photocatalytic degradation of X6G in the presence of slurry nanopowder TiO_2 (160 mg dm^{-3}) solution (▲) composite film without MC (■) composite film with MC (●) and without TiO_2 (×)

Table 2 Pseudo-first-order kinetic parameters of X6G diazo dye photocatalytic degradation

Material	Rate constant (min^{-1})	$t_{1/2}$ (min)
TiO_2 nanopowder	0.0547	12.67
Composite film with sol without MC	0.0231	30
Composite film with sol and MC	0.0277	25

To compare the photocatalytic degradation of composite TiO_2 films with nanopowder slurry, the dye solution was also decolorized in the presence of a dispersion of TiO_2 nanopowder with the same weight as film (0.0016 g = 160 mg dm^{-3}) and the results are represented in Fig. 9(▲). The rate constant for the slurry is greater than that of the two films, suggesting a considerably higher efficiency as photocatalyst. This may be due to limitations of reactant diffusion or it may be because only the external surface of the film samples is exposed to the pollutant solution, and therefore the effective area is much less than the (190–290 m^2/g) of the TiO_2 nanopowder. The results in Fig. 9(■ without MC and ● with MC) demonstrate that the rate constant for the composite film with MC is no worse and may be better than that of the film without MC. It is possible that an increased activity of the MC additioned film for photodegradation of X6G could result from greater porosity (as is seen in Fig. 7).

Conclusion

A nanocomposite TiO_2 film prepared from an anatase nano-powder and sol–gel derived titania has been demonstrated to have good film integrity, superior adhesion (measured by a scratch adhesion test) to films prepared from the nano-powder alone. The composite films showed a good photocatalytic activity for azo-dye degradation. The addition of methylcellulose led to more uniform films, with improved scratch resistance, without impairing the photocatalytic activity.

Acknowledgements The authors wish to thank the University of Isfahan for financially supporting this work. We wish to thank Kermanshah Oil Refinery for their partial support.

References

1. Claus H, Faber G, Koning H (2002) Appl Microbiol Biotechnol 59:672
2. Selvam K, Swaminathan K, Keo-Sang C (2003) World J Microbiol Biotechnol 19:591
3. Maguire RJ (1992) Water Sci Technol 25:265
4. Zhang C, Fu C, Bishop L, Kupferle M, Fitzgerald S, Jiang H, Harmer C (1995) J Hazard Mater 41:267
5. Chudgar RJ (1991) In: Kroschwits JI, Howe-Grant M (Eds) Kirk-Othmer encyclopedia of chemical technology, vol. 3. John Wiley & Sons Inc, New York
6. Pagga U, Taeger K (1994) Water Res 28:1051
7. Legrini O, Oliveros E, Braun AM (1993) Chem Rev 93:671
8. Hoffmann MR, Martin ST, Choi W, Bahnemann DW (1995) Chem Rev 95:69
9. Ollis DF, Al-Ekabi H (eds) (1993) Photocatalytic purification and treatment of water and air. Elsevier Science Publishers, Amsterdam
10. Turchi CS, Ollis DF (1990) J Catal 122:178
11. Fox MA, Dulay M (1993) Chem Rev 93:341
12. Wuhrmann K, Mechsner K, Kappeler T (1980) Euro J Appl Microbiol Biotechnol 9:325
13. Buechler KJ, Noble RD, Koval CA, Jacoby WA (1999) Ind Eng Chem Res 38:892
14. Konstantinou IK, Sakellarides TM, Sakkas VA, Albanis TA (2001) Environ Sci Technol 35:398
15. Habibi MH, Hassanzadeh A, Mahdavi S (2005) J Photochem Photobiol A: Chem 172:89
16. Habibi MH, Vosoghian H (2005) J Photochem Photobiol A: Chem 172:45
17. Habibi MH, Tangestaninejad S, Yadollahi B (2001) Appl Catal B: Environ 33:57
18. Yanagisawa K, Yamamoto Y, Feng Q, Yamasaki N (1998) J Mater Res 13:825
19. Chan CK, Porter JF, Li YG, Guo W, Chan CM (1999) J Am Ceram Soc 83:566
20. Yu JC, Yu JG, Ho WK, Jiang ZT, Zhang LZ (2002) Chem Mater 14:3808
21. Yasumori A, Shinoda H, Kameshima Y, Hayashi S, Okada K (2001) J Mater Chem 11:1253
22. Woolfrey JL, Bartlett JR (1998) In: Klein LC, Pope EJA, Sakka S, Woolfrey JL (eds) Sol–gel processing of advanced materials. The American Ceramic Society, p 3
23. Mackenzie JD (1986) In: Hench LL, Urlich DR (eds) Science of ceramic chemical processing, Wiley
24. Segal D (1997) J Mater Chem 7:1297
25. Bouquin O, Blanchard N, Colombian PH (1987) In: Vincenzini P (ed) High tech ceramics. Elsevier, Amsterdam
26. Livage J, Beteille F, Roux C, Chatry M, Davidson P (1998) Acta Mater 46:743
27. Brinker CJ, Scherer GW (1990) Sol–gel science – the physics and chemistry of sol–gel processing. Academic Press
28. Scherer GW (1990) J Am Ceram Soc 73:3
29. Scherer GW (1987) J Non-Cryst Solids 92:375
30. Ring TA (1996) Fundamentals of ceramic powder processing and synthesis. Academic Press
31. German RM (1996) Sintering theory and practice. Wiley, New York, p.67
32. Arabatzis IM, Antonaraki S, Stergiopoulos T, Hiskia A, Papaconstantinou E, Bernard MC, Falaras P (2002) J Photochem Photobiol A: Chem 149:237
33. Keshmiri M, Troczynski T, Mohseni M (2004) Appl Catal B: Environ 53:209
34. Bange K, Ottermann CR, Anderson O, Jeschkowsky U, Laube M, Feile R (1991) Thin Solid Films 197:279
35. Hossein-Babaei F, Keshmiri M, Kakavand M, Troczynski T (2005) Sensor Actuator B: Chem 110:28
36. Chatterjee D, Dasgupta S (2005) J Photochem Photobiol C: Photochem Rev 6:186
37. Chen W, Zhang J, Fang Q, Li S, Wu J, Li F, Jiang K (2004) Sensor Actuator B 100(1–2):195
38. Habibi MH, Talebian N (2007) Dyes Pigments 73:186

39. Habibi MH, Talebian N (2005) Acta Chim Slov 52:53
40. Hassanzadeh A, Habibi MH, Zeini Isfahani A (2004) Acta Chim Slov 51:507
41. Caruso RA, Schattka JH (2000) Adv Mater 24:1921
42. Lewis JA (2000) J Am Ceram Soc 83:2341
43. Okada K, Yamamoto N, Kameshima Y, Yasumori A (2001) J Am Ceram Soc 84:1591
44. Chen W, Tao X (2005) J Am Ceram Soc 88:2998
45. Mazzarino I, Piccinini P, Spinelli L (1999) Catal Today 48:315
46. Harizanov O, Harizanova A (2000) Solar Energy Mater Solar Cells 63:185
47. Yang TC-K, Wang S-F, Tsai SH-Y, Lin S-Y (2001) Appl Catal B: Environ 30:293
48. Houas A, Lachheb H, Ksibi M, Elaloui E, Guillard C, Herrmann JM (2001) Appl Catal B: Environ 31:145
49. Fujishima A, Rao TN, Tryk DA (2000) J Photochem Photobiol C: Photochem Rev 1:1–21